THE ELECTRIC FIELD INSTRUMENT ON THE POLAR SATELLITE

P. HARVEY, F. S. MOZER,* D. PANKOW and J. WYGANT**
Space Sciences Laboratory, University of California, Berkeley, U.S.A.

N.C. MAYNARD,*** H. SINGER‡ and W. SULLIVAN
Phillips Laboratory, Geophysics Directorate/GPSG, Hanscom Air Force Base, U.S.A.

P.B. ANDERSON
Center for Space Physics, Boston University, MA, U.S.A.

R. PFAFF and T. AGGSON
NASA Goddard Space Flight Center, Greenbelt, MD, U.S.A.

A. PEDERSEN
European Space and Technology Center, Noordwijk, The Netherlands

C.-G. FÄLTHAMMAR
Royal Institute of Technology, Stockholm, Sweden

and

P. TANSKANNEN
University of Oulu, Oulu, Finland

(Received 19 February, 1993)

Abstract. The Polar satellite carries a system of four wire booms in the spacecraft spin plane and two rigid booms along the spin axis. Each of the booms has a spherical sensor at its tip along with nearby guard and stub surfaces whose potentials relative to that of their sphere are controlled by associated electronics. The potential differences between opposite sphere pairs are measured to yield the three components of the DC to >1 MHz electric field. Spheres can also be operated in a mode in which their collected current is measured to give information on the plasma density and its fluctuations. The scientific studies to be performed by this experiment as well as the mechanical and electrical properties of the detector system are described.

1. Introduction

The Electric Field Instrument (EFI) on the Polar spacecraft measures the three components of the ambient vector electric field and the thermal electron density. The results are used to study:

– Parallel and perpendicular electric fields and density variations in double layers, electrostatic shocks, and other spatially confined structures found in the auroral acceleration region and at other locations along the Polar orbit.

* Also at Physics Department, University of California, Berkeley, CA 94720, U.S.A
** Now at Tate Laboratory of Physics, School of Physics and Astronomy, University of Minnesota, 116 Church Street, S.E., Minneapolis, MN 55455, U.S.A.
*** Now at Mission Research Corporation, One Tara Blvd., Suite 302, Nashua, NH 03062, U.S.A.
‡ Now at NOAA R/E/SE, 325 Broadway, Boulder, CO 80303, U.S.A.

Space Science Reviews **71:** 583–596, 1995.

– The high-latitude convection electric field. The electric field and plasma density structure on field lines connected to the high-latitude magnetopause, polar cusp, and plasma mantle.

– Correlations of electric fields with those measured by other ISTP spacecraft at different points along the same magnetic field line or along a common boundary, or in different regions of the magnetosphere.

– Modes, phase velocities, and wavelengths of propagating waves and spatial structures.

The electric field and plasma density measurements are made over a frequency range of DC to above 20 kHz. The dynamic range of the electric field measurement is 0.02 to 1000 mV m^{-1}, while the plasma density will be measured at least over the range of 0.01 to 100 particles per cubic centimeter. A by-product of the experiment is measurement of the floating potential of the spacecraft over the range of about +1 to +90 V. Over this range, the density varies from less than 0.01 to more than 10 particles per cubic centimeter.

An important component of the Electric Field Instrument is a two-megabyte burst memory that allows storage of high-time-resolution field and plasma density measurements, allowing study of rapid variations of non-linear spatial structures and waves.

The EFI sensors are arranged as three orthogonal sphere pairs whose potential differences and Langmuir probe characteristics are measured. As illustrated in Figure 1, two of these sphere pairs are in the satellite spin plane on the ends of wire booms that provide tip-to-tip sphere separations of 100 and 130 m, respectively, while the third pair is aligned along the spacecraft spin axis with a 13.8 m tip-to-tip separation that is provided by rigid stacer booms.

The electric field preamplifiers have frequency responses to above one MHz to accommodate their use by the Plasma Wave Instrument. In addition, the Electric Field Instrument interfaces on the spacecraft with the Magnetic Field Experiment (which provides information that may be used to trigger bursts of data collection), and the Hydra and Tide plasma experiments (in order to coordinate simultaneous high-time-resolution data collection).

The heritage of the Electric Field Instrument encompasses instruments previously flown on the S3-3, GEOS, ISEE-1, *Viking*, CRRES, and *Freja* satellites, as well as experiments being built for FAST and Cluster.

Table I presents a summary of the weight and power consumption of the components of the Electric Field Instrument on the Polar spacecraft.

2. Scientific Discussion

Some of the scientific studies that will be performed with data obtained by the Electric Field Instrument are described below:

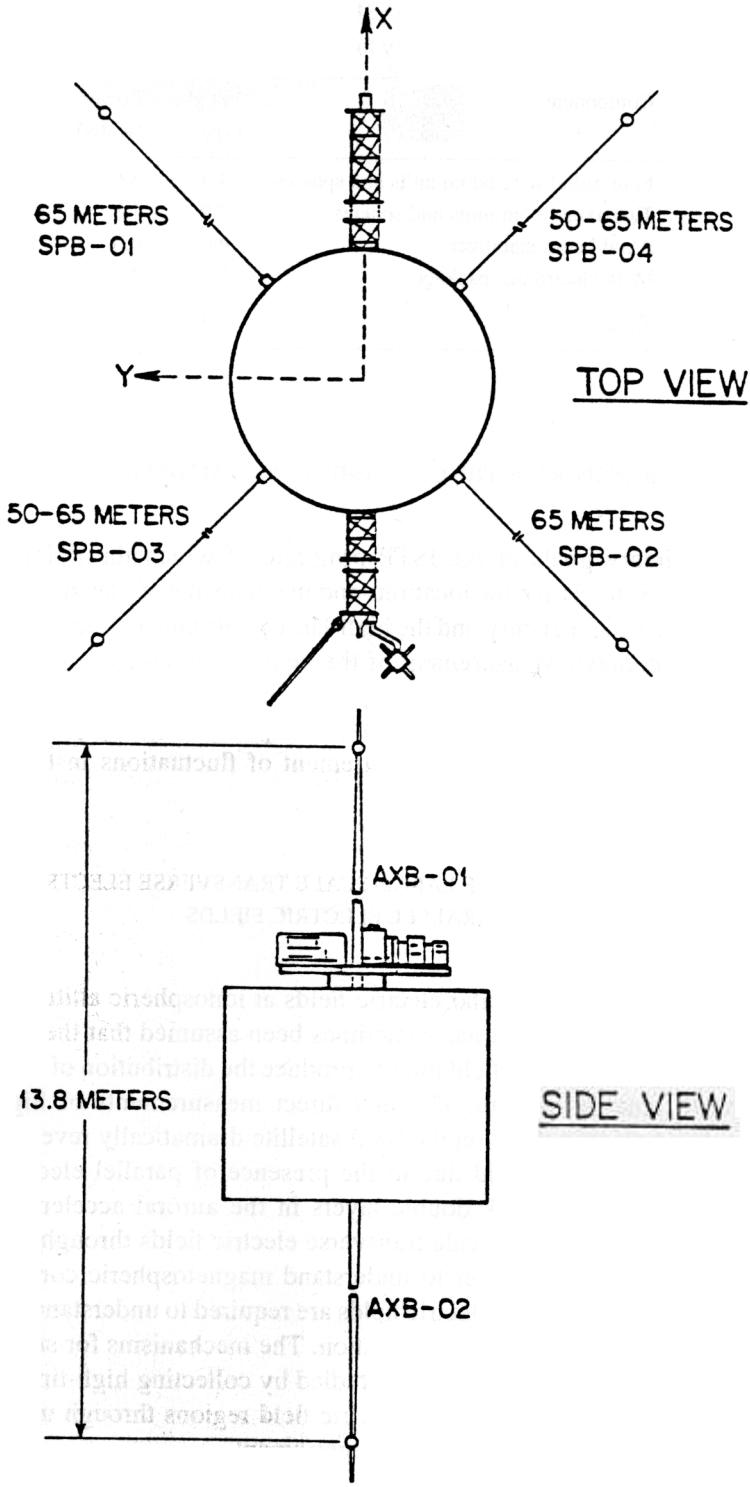

Fig. 1. Schematic drawing of the polar satellite, illustrating the wire booms.

TABLE I
Weight and power summary for the electric field instrument

Component	Weight (kg)	Power (watts)
Four radial wire boom units and spheres	14.3	
Two axial boom units and spheres	7.9	
Axial boom stabilizer	4.0	
Main electronics package	7.1	
Total	33.3	

2.1. PLASMA TRANSPORT IN THE CUSP AND PLASMA MANTLE

One of the primary goals of the ISTP program, of which the Polar satellite is one component, is to clarify the locations and mechanisms of plasma entry into the magnetosphere. The polar cusp and the high-latitude plasma mantle are of particular interest in this context. Measurement of the quasi-static electric field will reveal the plasma flow and transport in these regions, and show how the transport varies with solar wind conditions. If eddy diffusion of plasma is an important transport mechanism, this will be seen by measurement of fluctuations in the transverse electric field.

2.2. ALTITUDE DEPENDENCE OF LARGE-SCALE TRANSVERSE ELECTRIC FIELDS AND OBSERVATIONS OF PARALLEL ELECTRIC FIELDS

The distribution of perpendicular electric fields at ionospheric altitudes has been well established. In the past it has sometimes been assumed that these fields map along equipotential magnetic field lines to produce the distribution of electric fields throughout the magnetosphere. The first direct measurements of high-latitude, magnetospheric electric fields on the S3-3 satellite dramatically revealed that this mapping assumption is invalid due to the presence of parallel electric fields in electrostatic shocks and weak double layers in the auroral acceleration region. Thus, measurements of large-scale transverse electric fields throughout the magnetosphere are required in order to understand magnetospheric convection, and direct observations of parallel electric fields are required to understand the location and extent of regions of particle acceleration. The mechanisms for supporting the observed parallel electric fields will be studied by collecting high-time-resolution data on the microphysics of parallel electric field regions through use of the on-board burst memory in the Electric Field Instrument.

2.3. Electric fields of ULF waves

Measurements of ULF electric fields at low and modest magnetic latitudes have been made on spacecraft such as ISEE-1 and GEOS. Examples of electric field fluctuations both with and without accompanying magnetic field fluctuations have been observed, indicating that both electrostatic and electromagnetic modes exist at such frequencies. These measurements will be complemented by wavelength measurements of the same phenomena on Polar and by extending such observations to the high-altitude, high-latitude region.

2.4. Substorm electric fields at high latitudes

Substorms are associated with large, transient, inductive electric fields which are responsible for many of their features, including enhanced electric currents, particle precipitation, and plasma injection. At low and moderate latitudes these fields have been measured by ISEE-1 and GEOS. An important issue is the character of these fields at high latitude, and measurements are required on time scales as short as the local ion gyroperiod.

Another substorm-related question is the extent of penetration of the associated electric fields into the plasmasphere. Combined measurements of electric fields on Polar and Geotail will answer this question.

2.5. Fine structure and time variations

Electric field experiments on S3-3, ISEE, and GEOS have seen large electric fields associated with fine structure in all regions of the magnetosphere, including the neutral sheet, the high-latitude boundary layer, the acceleration region, and the bow shock. Many of these structures look like weak double layers although the time resolution has not been sufficient to draw definitive conclusions. The Electric Field Instrument on Polar, with its burst memory, possesses sufficient time resolution to decide this matter and to explore a new region of space in which instabilities and non-linear processes may produce similar phenomena.

2.6. Modes, phase velocities, and wavelengths of waves and spatial structures

Wavelengths of tens to hundreds of meters may be measured by analyzing the ratio of the responses of the three electric field antennas of different lengths. The mode, phase velocity, and wavelengths of electrostatic waves may be estimated from the ratio of the measured electric fields to the density fluctuations. The phase velocity of traveling waves and the motions of spatial structures may be determined by the time delay of their responses on the different spheres. Lastly, the field components and the plasma density fluctuations recorded in the on-board

burst memory can yield information on non-linear processes through their auto-correlations, bi-correlations, and tri-correlations.

2.7. HIGH-TIME-RESOLUTION MEASUREMENTS OF PLASMA SENSITY

Since both the measured spacecraft floating potential and the measured current to a voltage-biased sphere depend on the plasma density, relative density variations on time scales of less than one millisecond or spatial scales of a few meters will be obtained. This data will be used in the study of density cavities, spatial turbulence, particle acceleration regions, etc.

3. Electronic Design

A simplified block diagram of the EFI system electronics is given in Figure 2. Circuits are contained in each of the six spheres and boom units as well as in the main electronics package. The major components of this block diagram will be discussed by following the signal from the sensors to the data outputs.

The first electrical interface is between the sensors and the surrounding space plasma. Each spherical sensor is surrounded by a pair of stubs that are electrically connected to each other and a pair of guards that are also connected to each other (see Figure 3). The potentials on the guards and stubs are offset from their associated sphere potential by values that may be commanded from the ground. These values are determined from on-board diagnostic experiments that seek to minimize the flow of photoelectrons between the sphere and the stubs, guards, and wire that runs from the guard to the spacecraft (see Figure 3). Typical values of these offset voltages are less than one volt for the stubs and -3 to -9 V for the guards. The stub offset voltage compensates for the difference of the work functions of the sphere and the stubs, such that the surfaces of the two conductors are at the same potential and the net photocurrent from one to the other is zero. The guard potential decelerates and stops photoelectrons that would otherwise flow from the sphere assembly to the spacecraft or vice-versa.

Block diagrams of the sphere preamplifier in the voltage mode (when the potential of a current-biased sphere is being measured) and the current mode (when the current to a voltage-biased sphere is being measured) are given in Figures 4 and 5. The stub and guard voltages are illustrated schematically in these figures as two variable batteries. An additional variable battery voltage in Figures 4 and 5 serves to current-bias the spheres in the voltage mode and to voltage-bias the spheres in the current mode. Since this voltage is referenced to the sphere output potential in the voltage mode, a current equal to the variable voltage divided by a fixed resistance is placed on the spheres in this mode. This current may be varied from about -500 to $+500$ nanoamperes by software control. In the current mode, the variable voltage between -40 and $+40$ V appears on the sphere. It may be stepped

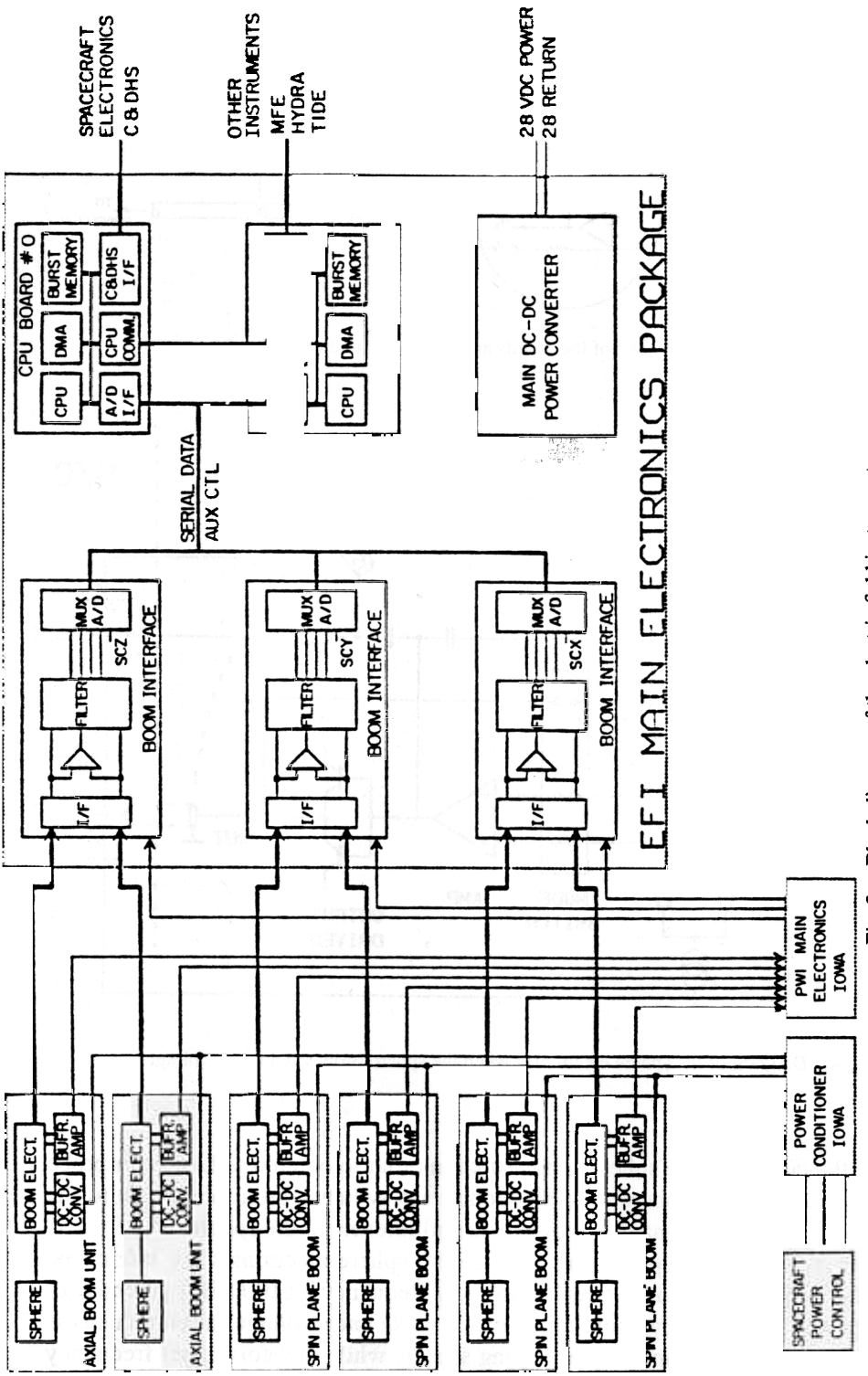

Fig. 2. Block diagram of the electric field instrument.

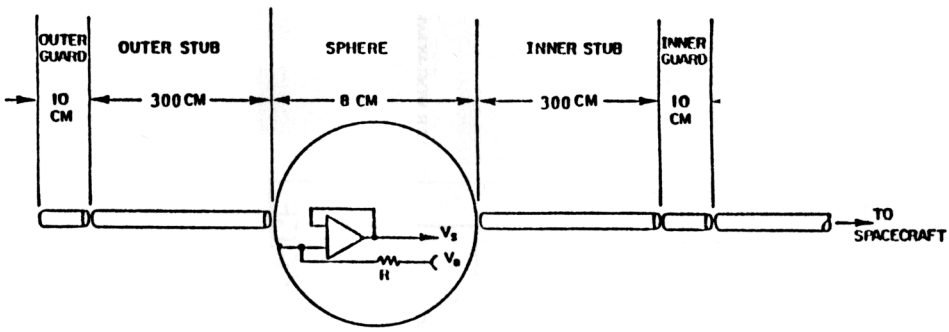

Fig. 3. Schematic of the guards and stubs surrounding each sphere.

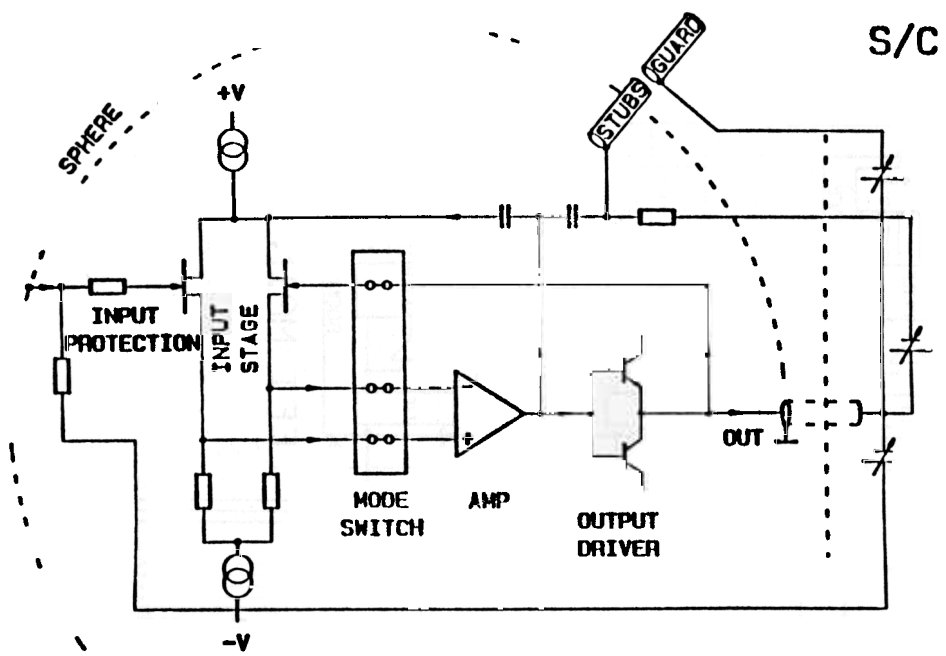

Fig. 4. Diagram of the sphere electronics when the sphere is operated in the voltage mode.

while the current to the sphere is measured in order to obtain the Langmuir probe characteristic of the sphere. The electronics are switched from one mode to the other by a ground command that activates multiplexers in the spheres.

The 12-V power supplies that operate the sphere electronics are referenced to a floating ground that is equal to the low-frequency (<1000 Hz) potential of the sphere. Thus, the dynamic range of low-frequency voltage measurements is equal to the 100-V range of the floating supply, while that for higher frequency

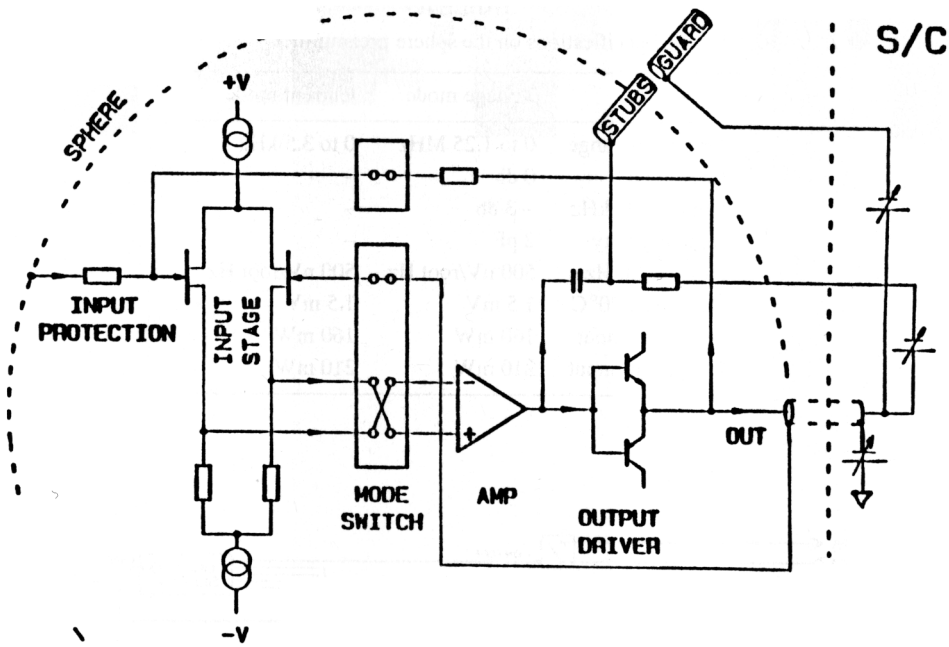

Fig. 5. Diagram of the sphere electronics when the sphere is operated in the current mode.

measurements is the 12-V power supply rails. Separate DC-DC converters are provided for each sphere to increase reliability through redundancy.

The gain versus frequency of the sphere preamplifiers depends on plasma parameters because the sheath capacitance depends on the Debye length and the signal in the plasma is attenuated by the ratio of the electronic input capacitance to the sheath capacitance. For typical conditions, the unity gain low frequency response decreases by about 3 db above a frequency of about 1 to 10 kHz. Sphere pairs were matched such that the difference in gain between opposite pairs was typically less than 0.1 db at all frequencies below 700 kHz and the phase difference of the outputs from opposite spheres was less than 4 deg. Additional specifications on the sphere preamplifiers are given in Table II.

A block diagram of the remainder of the electronics in each boom unit is given in Figure 6. The serial DACs receive eight-bit digital inputs from the main electronics and their analog outputs determine the voltages on the guards and stubs, and the voltage or current bias. The remainder of the electronics in the boom units provide the 12- and 100-V power, interface the sphere output to the Plasma Wave Instrument, command the sphere preamplifier into either the current or voltage mode, drive deployment motors in the radial booms, and provide status information on the boom operation. As illustrated in Figure 2, the main electronics package contains three boom interface boards, two CPU boards, and a power

TABLE II

Specifications on the sphere preamplifier

	Voltage mode	Current mode
Frequency range		0 to 3.5 kHz
Gain at DC		
Gain at 700 kHz		
Input capacity		–
Noise at 20 Hz		500 nV/root Hz
DC offset, 70°C		1.5 mV
Power, no input		160 mW
Power, full input		210 mW

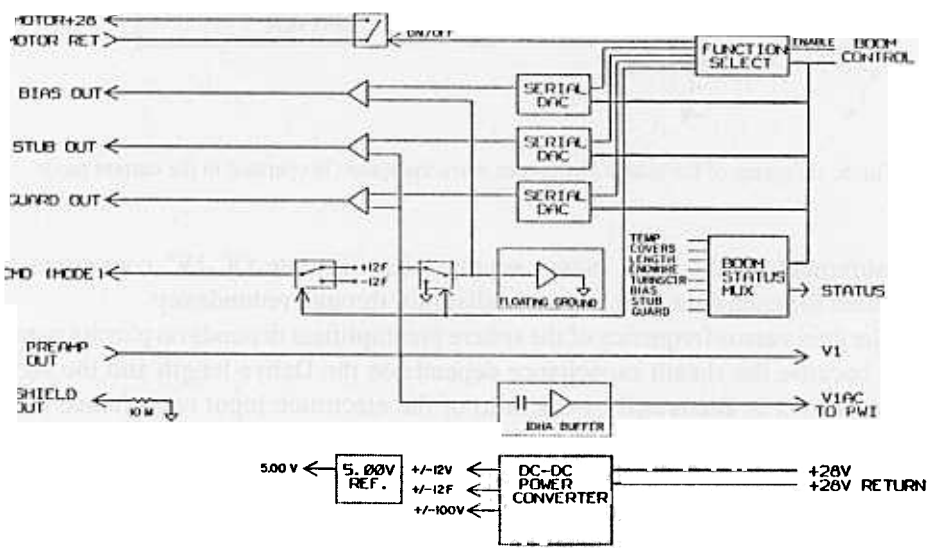

Fig. 6. Block diagram of the boom unit electronics.

supply. A block diagram of a boom interface board is given in Figure 7. Each boom interface board accepts analog inputs from one pair of spheres and one component of the search coil magnetometer provided by the Plasma Wave Instrument. (Since the interfaces between EFI and the Magnetic Field Experiment, Tide, and Hydra, are digital, as indicated in Figure 2, they are not part of the boom interface board.) For each sphere pair, eleven electric field analog outputs are produced by passing the sphere inputs through filtering and difference circuits. In the voltage mode, these eleven outputs are:

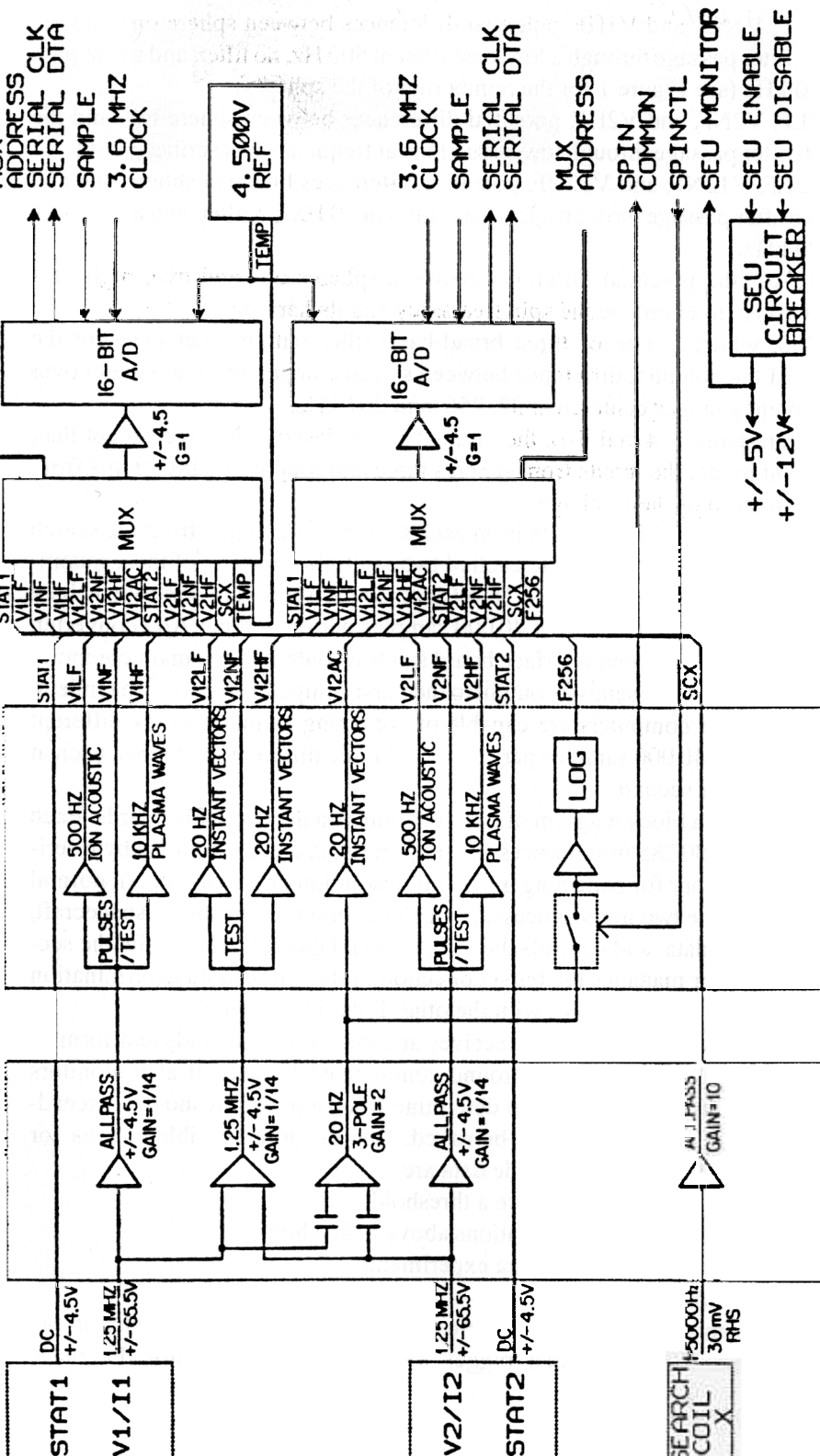

Fig. 7. Block diagram of a boom interface electronics board.

– V1LF, V1NF, and V1HF, potential differences between sphere one and the spacecraft after passage through a low-pass filter at 500 Hz, no filter, and a low-pass filter at 10 kHz (see Figure 1 for the numbering of the spheres).

– V2LF, V2NF, and V2HF, potential differences between sphere two and the spacecraft after passage through low-pass filters at frequencies described above.

– V12LF, V12NF, and V12HF, potential differences between sphere one and sphere two after passage through a low-pass filter at 20 Hz, no filter, and a low-pass filter at 20 kHz.

– V12AC, the potential difference between spheres one and two, high-pass filtered at 20 Hz to eliminate the spin frequency and its harmonics.

– F256, which is one of three broad-band filter outputs that measure the amplitude of the potential difference between selected opposing sphere pairs over broad frequency ranges centered at 32, 256, and 2048 Hz.

For sphere-pairs 3–4 and 5–6, the outputs are as described above except that, in the current mode, the inputs from spheres three and four are their currents from the plasma instead of their voltages.

The eleven electric field outputs from each sphere pair and that from the search coil magnetometer are connected to each of two multiplexers. Any of these quantities may be selected and digitized to 16-bit accuracy at a software controlled clock rate less than the maximum rate of 40 000 samples per second per A/D converter. One converter on each boom interface board sends its output to the main computer while the other converter sends its output to the burst computer. Working in tandem, the main and burst computers are capable of collecting as many as six different quantities, each at 40 000 samples per second, or three different quantities, each at 80 000 samples per second.

Figure 8 shows a block diagram of the electronics on the two CPU boards. Each board contains an 80C85 microprocessor, support logic, and a one-megabyte serially accessed memory for collecting high-time-resolution bursts of data. In normal operation, one of the two microprocessors receives commands from the spacecraft, formats telemetry data, and controls the bias, stub and guard DACs, while the second microprocessor manages the burst collection of data, threshold determination and event-triggers, and interfaces with the other Polar instruments.

Software in the microprocessors receives and decodes commands and formats data for telemetry in table-driven, ground-commanded formats. It also monitors electric field or magnetic field data to determine when a burst threshold is exceeded and burst data collection should be saved. One or more possible criteria for triggering the collection of burst mode data are:

– One or more filter outputs above a threshold.
– DC magnetic field or its fluctuations above a threshold.
– Trigger received from the Hydra experiment.
– Ground command.

The burst memory may be divided into two or more parts and operated in the following fashion. Each time that a 'bigger' event is observed, it is stored in place

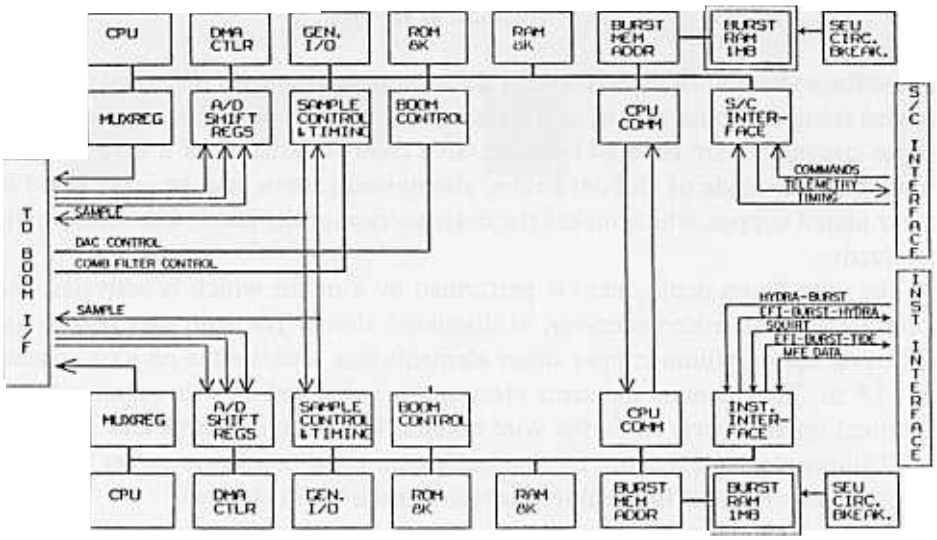

Fig. 8. Block diagram of the two CPU electronics boards.

of the smallest of the previously stored events. In this way, the 'best' events of the previous time period are accumulated in burst memory. Since the parameters of the trigger algorithm are controlled by ground command, the operation of the trigger will be determined by experience and the science that is desired. For example, to study Langmuir turbulence, the highest frequency electric field amplitude might serve as the trigger and each increase of this amplitude by more than 25% over the threshold for the previous recording might trigger collection of a new burst. Data from the burst memory are transmitted to ground by pre-empting part of the normal telemetry stream for this purpose.

Other functions performed by the flight software are:

– On-board, sine wave, least-squares fits of potential differences between opposite sphere pairs, in order to determine electric field components in the spin plane. These fits are always in the telemetry stream, independent of the operating mode of the instrument.

– Bias sweeps. In the voltage mode the bias current to the spheres may be swept and the resulting data analyzed to determine the optimum bias current, which is the current that minimizes the sheath impedance. In the current mode, the voltage on the spheres may be swept in order to measure the Langmuir probe characteristic and deduce the plasma density and temperature.

– Deployment. The spin-plane boom deployment sequence is controlled by the on-board microprocessor which, among other things, temporarily stops the deployment of one sphere of a pair if its deployed length becomes greater than that of its mate by more than about 20 centimeters. The axial boom deployment is accomplished by firing release pyrotechnics through the spacecraft electronics.

4. Mechanical Design

The voltages required and produced by the sphere electronics of Figures 4 and 5 are carried along the boom wire by eight conductors that surround a coaxial signal line. These conductors are covered by successive layers consisting of a load carrying braid which is made of DuPont kevlar, aluminized kapton, and an outer braid of silver plated copper, which makes the outer surface of the boom wire electrically conductive.

The wire boom deployment is performed by a motor which is activated and controlled by the microprocessor, as discussed above. The spin axis booms are rigid, pop up, beryllium-copper stacer elements that separate the on-axis spheres by 13.8 m. They contain the same electronics, guard and stub arrangement, and electrical interconnects as do the wire booms. The on-axis guards and stubs are small stacer elements that are mechanically connected to a larger stacer that provides the major part of the deployed length of each boom element.

As part of the on-axis boom system, an axial boom stabilizer is provided. This is an approximately 1.98 m tall conical section made of composite materials, inside of which the axial boom deployment mechanisms reside.

5. On-Orbit Operations

Following launch, the wire booms will be deployed over a period of several days with science stops interspersed for performing diagnostic experiments to measure spacecraft associated fields as a function of distance from the spacecraft. Following this deployment, the separation between wire boom pairs will be 100 m for one pair and 130 m for the other. The purposes of different boom lengths are to verify that the DC signal is proportional to the boom length and to obtain wavelength information on short wavelength modes from the different response of the two antennas. Approximately a year following launch, the shorter antennas may be deployed to their full 130 m tip-to-tip length.

Additional on-orbit decisions will be made on which spheres are operated in the current mode and how often they are operated in this way. The nominal plan is to operate spheres 3 and 4 (on the shorter wire booms) in the current mode approximately 25–50% of the time and to operate the remaining spheres in the voltage mode only.

Acknowledgement

This work was performed under NASA contract NAS5-30367.